Malaysian Journal of Analytical Sciences (MJAS)
Published by Malaysian Analytical Sciences Society

PHOTOCATALYTIC DEGRADATION OF OFLOXACIN ANTIBIOTIC BY g-C_3N_4/ZnO NANOCOMPOSITE UNDER VISIBLE LIGHT IRRADIATION

(Fotokatalitik Degradasi Ofloksasin Antibiotik oleh Nanokomposit g-C_3N_4/ZnO di Bawah Penyinaran Cahaya Tampak)

Nor Fadilah Chayed[1,2], Salma Izati Sinar Mashuri[1,2], Izzati Shafiqah Zainal Abidin[1,2], Muhd Firdaus Kasim[1,2], Noor Haida Mohd Kaus[4], Mohd Sufri Mastuli[1,2], Umer Rashid[5], and Mohd Lokman Ibrahim[1,2,3*]

[1]Centre for Functional Materials and Nanotechnology,
Institute of Science, Universiti Teknologi MARA, 40450 Shah Alam, Selangor, Malaysia
[2]School of Chemistry and Environment,
Faculty of Applied Sciences,
Universiti Teknologi MARA, 40450 Shah Alam, Selangor, Malaysia
[3]Industrial Waste Conversion Technology,
Universiti Teknologi MARA, 40450 Shah Alam, Selangor, Malaysia
[4]School of Chemical Sciences,
Universiti Sains Malaysia, 11800 Penang, Malaysia
[5]Institute of Nanoscience and Nanotechnology,
Universiti Putra Malaysia, 43400 Serdang Selangor, Malaysia

[*]Corresponding author: mohd_lokman@uitm.edu.my

Received: 15 September 2023; Accepted: 29 October 2023; Published: 29 December 2023

Abstract

A critical global environmental crisis has emerged due to the use of synthetic organic pollutants in industry, which resulted in the pollution of water. Recently, photocatalysis has attracted much attention for its potential to effectively, economically, and environmentally friendly remove organic pollutants from wastewater. ZnO is known as a potential photocatalyst for the degradation of wastewater in the UV region. However, ZnO has limited light absorption within the UV region and exhibits fast recombination of electron-hole pairs, which reduces its efficiency. To overcome this issue, a g-C_3N_4/ZnO photocatalyst for organic pollutant degradation in wastewater was developed to extend the light absorption towards the visible region. This research aims to investigate the performance of g-C_3N_4/ZnO nanocomposites in the degradation of ofloxacin (OFL). The ZnO was prepared using the sol-gel method, while the g-C_3N_4 was prepared using thermal decomposition. The composite catalyst of g-C_3N_4/ZnO was prepared by mixing g-C_3N_4 and ZnO. The prepared catalysts were characterized using X-ray diffraction (XRD), field emission scanning electron microscopy (FESEM), UV-Vis NIR spectrophotometer, high-resolution transmission electron microscopy (HRTEM), and Brunauer Emmet Teller (BET). As a result of the composite photocatalyst combining ZnO and g-C_3N_4, the band gap decreased from 3.30 eV to 2.92 eV. The degradation of OFL using g-C_3N_4/ZnO nanocomposite is 11 times higher than that of pristine ZnO and double than that of pristine g-C_3N_4.

Keywords: g-C_3N_4/ZnO, ofloxacin, degradation, photocatalysis, wastewater treatment

Abstrak

Krisis alam sekitar global yang kritikal telah muncul akibat penggunaan bahan pencemar organik sintetik di dalam industri, mengakibatkan pencemaran air. Baru-baru ini, fotokatalisis telah menarik banyak perhatian kerana potensinya untuk merawat bahan organik daripada air sisa tercemar secara berkesan, ekonomikal dan mesra alam. ZnO dikenali sebagai fotomangkin berpotensi untuk degradasi air sisa tercemar di kawasan UV. Walau bagaimanapun, ZnO mempunyai penyerapan cahaya yang terhad dalam kawasan UV hanya disebabkan oleh tenaga jurang jalur yang besar (3.37 eV) dan mempamerkan penggabungan semula pantas pasangan lubang elektron, yang mengurangkan kecekapannya. Untuk mengatasi isu ini, fotomangkin g-C_3N_4/ZnO untuk degradasi bahan organik dalam rawatan air sisa telah dihasilkan untuk meningkatkan penyerapan cahaya ke arah cahaya tampak. Matlamat penyelidikan ini adalah untuk menyiasat prestasi nanokomposit g-C_3N_4/ZnO dalam degradasi ofloksasin (OFL). ZnO disediakan menggunakan kaedah sol-gel, manakala g-C_3N_4 disediakan menggunakan penguraian terma. Mangkin komposit g-C_3N_4/ZnO disediakan dengan mencampurkan g-C_3N_4 dan ZnO. Pemangkin yang disediakan telah dicirikan menggunakan pembelauan sinar-X-(XRD), mikroskopi imbasan elektron pancaran medan (FESEM), spektrofotometer UV-Vis NIR, mikroskopi transmisi elektron resolusi tinggi (HRTEM), dan Brunauer Emmet Teller (BET). Hasil daripada fotomangkin komposit yang menggabungkan ZnO dan g-C_3N_4, jurang jalur menurun daripada 3.30 eV kepada 2.92 eV. Degradasi ofloksasin menggunakan nanokomposit g-C_3N_4/ZnO adalah 11 kali lebih tinggi daripada ZnO dan 2 kali lebih tinggi daripada g-C_3N_4 tulen.

Kata kunci: g-C_3N_4/ZnO, ofloksasin, degradasi, fotokatalisis, rawatan air tercemar

Introduction

The increasing use of pharmaceuticals in recent years has attracted researchers' attention due to their harmful impact on the environment. They have been identified as the most common organic pollutants found in wastewater from various sources, such as hospitals, households, industries, and agricultural waste. Antibiotics contribute to a large proportion of the numerous pharmaceutical products consumed due to their widespread use in veterinary and human medicine for the treatment or prevention of bacterial diseases [1, 2]. Ofloxacin (OFL) is a quinolone antibiotic known as an antibacterial agent used for the treatment of bacterial infections in body parts including the skin, kidney, soft tissue, respiratory tract, and urine tract [3]. OFL is a third-generation fluoroquinolone antibiotic and cannot be completely metabolized by the human body, in which 20-80% of the indigested agent is excreted in pharmacologically active form. It has been reported that low concentrations of OFL can accumulate in water for prolonged periods of time. The fluoroquinolones that are present in wastewater can lead to the proliferation of drug resistant bacteria through induction and selection. It can be harmful to human health and can potentially reduce the ability of human immune system to fight those bacteria strains [4–9].

OFL has been detected in water environments such as in hospital wastewater (35 µg/L), urban wastewater treatment plants (1.8 µg/L), sewage water (0.89-31.73 µg/L) and surface water (0.5-35 µg/L) [10,11]. Various methods have been extensively explored for the removal of OFL such as adsorption, biodegradation, chlorination, precipitation, coagulation etc. [6, 12-15]. However, most of the methods are unable to remove the organic pollutant completely and effectively. In recent years, photocatalysis has attracted attention for antibiotic degradation due to its high efficiency, excellent stability, and eco-friendliness compare to the conventional methods [5, 16, 17].

ZnO is a metal oxide semiconductor that has good electron transfer ability, exhibits photostability and can generate holes for strong oxidation. Despite its numerous advantages, ZnO has certain limitation of poor photocatalytic response to visible light due to having a wide band gap (3.37 eV) and fast recombination of photogenerated electron-hole pairs [18, 19]. Various approaches have been attempted to overcome this limitation, which include making suitable composites such as ZnO/CdS, ZnO/Sn_3O_4, CuO/ZnO, ZnO/TiO_2, ZnO-CoO_x-CeO_2 and etc. [20-24].

Graphitic carbon nitride (g-C_3N_4) is the most stable allotrope of carbon nitrides at ambient temperature and has received a lot of attention in recent years. The g-C_3N_4 is a metal-free n-type semiconductor polymer with a two-dimensional structure similar to graphite. In

the visible spectral range, g-C_3N_4 has a band gap of 2.7 eV, corresponding to an optical wavelength of 460 nm, making it an excellent photocatalyst. In addition to being safe and non-toxic, g-C_3N_4 is highly stable and has a strong reduction ability, as well as being light active. [25-29]. However, g-C_3N_4 also has disadvantages of photogenerated electron and holes pairs that easily recombine, which greatly reduces the performance of the photocatalyst. Since g-C_3N_4 has a large resistance, it blocks the transfer of photoexcited electrons.

The combination of g-C_3N_4/ZnO could improve the photocatalytic performance due to the complementary properties of both g-C_3N_4 and ZnO. The ability of g-C_3N_4 to absorb visible light is well known, whereas ZnO can absorb only UV light. This combination can extend the light absorption with a broader spectrum of light that can enhance the photocatalytic performance. The g-C_3N_4/ZnO composite exhibits synergistic effects, resulting in a more efficient and effective photocatalyst than either material alone. This synergy has the potential to improve electron-hole pair generation and separation which can improve the photocatalytic performance [30-33]. The formation of g-C_3N_4 and ZnO to form a heterojunction can significantly reduce the recombination rate of electron holes by modifying the charge carrier pathway at the interface. Hybrid structures can facilitate interfacial charge transfer, enabling electrons and holes to be simultaneously available for selective redox reactions [34]. In summary, heterojunction of g-C_3N_4 and ZnO provides several advantages, including improved charge separation, extended light absorption range, increased photocatalytic activity, and improved stability. Due to these characteristics, g-C_3N_4/ZnO heterojunctions are attractive for a variety of environmental and energy applications.

In the present work, g-C_3N_4/ZnO nanocomposite has been synthesized using sol-gel, thermal decomposition method followed by wet impregnation method. The photocatalytic activity was evaluated based on the degradation of OFL. It has been observed that the photocatalytic activity of the composite has improved significantly compared to the pristine.

Materials and Methods

Materials

Melamine ($C_3H_6N_6$,>99%) was used as the precursor for g-C_3N_4, Zinc acetate $Zn(CH_3COO)_2$ was used for the preparation of ZnO. The ammonium hydroxide (NH_4OH) and absolute ethanol were used as the solvent, and analytical grade of OFL (Sigma-Aldrich) was used as the organic pollutant in this study.

Preparation of the g-C_3N_4/ZnO photocatalysts

The synthesis method that was used for the preparation of ZnO catalyst is the sol-gel method. This method involves the dissolution of the starting material, $Zn(CH_3COO)_2$, in absolute ethanol. The solution was then stirred using a magnetic stirrer for an hour to make sure the solution completely dissolved and obtained a homogenous mixture. The NH_4OH, was then added to the solution to obtain pH 9. The mixture was then dried to obtain the ZnO precursor. The ZnO precursor was then annealed at 300 °C for 24 hours. The g-C_3N_4 was prepared using thermal decomposition by directly heating the melamine using a crucible and covering it with a lid at 550 °C for 3 hours. The preparation of a composite catalyst of g-C_3N_4/ZnO was done by using wet impregnation, which involved mixing g-C_3N_4 and ZnO in a 1:1 mass ratio. The solid mixture was then dissolved in deionized water and stirred for 1 hour to obtain a homogenous solution. The mixture solution was then filtered, washed with deionized water, and dried in an oven at 200 °C for 5 hours. The dry powder was then ground into a very fine powder to obtain the final products, which were ready for other characterizations.

Characterization of the g-C_3N_4/ZnO photocatalysts

The phase studies of the catalyst were performed by the XRD PANalytical X'Pert Pro MPD Diffractometer using the Bragg Brentano optical configuration under ambient conditions. The morphology and crystallite size of the photocatalysts were examined using field emission scanning electron microscopy (FESEM, JEOL JSM-7600F) equipped with energy dispersive X-ray spectroscopy (EDX) to give quantitative elemental mapping. The light absorption properties were studied using the Perkin Elmer Lambda 950 UV-Vis NIR in

reflectance mode. The surface area, pore volume, and pore diameter were determined using the N_2 adsorption-desorption isotherm by the BELJAPAN BELSORP-mini porosity analyzer.

Degradation of OFL by g-C_3N_4/ZnO

The photocatalytic activity of ZnO, g-C_3N_4, and g-C_3N_4/ZnO photocatalyst was evaluated by the determination of OFL degradation at each interval using UV-Vis NIR spectrophotometer. The photocatalytic reactor is equipped with a 150-watt LED visible lamp as the light source to carry out the photocatalytic activity (under standard temperature and pressure). The amount of 0.25 g of photocatalyst was added to 150 mL of 10 ppm OFL solution. Then, the solution was stirred for about 30 minutes in a dark condition for equilibrium adsorption, and then the light source was applied until the reaction was completed. The solution was extracted at intervals of 15 minutes. The photocatalytic analysis was performed using UV-Vis NIR spectrophotometer in absorbance mode. The photocatalytic performance of the photocatalyst was evaluated through the degradation of OFL using the following equation [1]:

$$Degradation\ (\%) = \frac{Co - Ct}{Co} \times 100\% \qquad (1)$$

where C_0 is the initial concentration of pollutant and C_t is the concentration of OFL at time (min).

Results and Discussion

Figure 1 represents the XRD patterns of pure ZnO, g-C_3N_4, and composite g-C_3N_4/ZnO. The phase structure was analyzed by the XRD Xpert Highscore Plus software. The 2θ values that correspond to the diffraction peak of the ZnO sample are 31.7°, 34.4°, 36.2°, 47.3°, 56.5°, 62.7°, 66.4°, 67.9°, and 69.0°, corresponding to (100), (002), (101), (102), (110), (103), (200), (112), (201), (004), (202), and (104) planes, which prove that the sample is pure and belongs to the hexagonal wurtzite crystalline phase of ZnO (ICDD No. 01-079-2205). The XRD pattern of g-C_3N_4 shows two peaks at 13.1° and 27.4°, which correspond to the ICDD pattern of g-C_3N_4 (ICDD No. 01-087-1526). The 13.1° peak that corresponds to the (100) plane indicates the periodic arrangement of the structural units in the layer that is graphite-like phase carbon nitride. The intensive peak at 27.4° belongs to the (002) plane and corresponds to the interlayer stacking of the conjugated carbocyclic plane [33]. The position of these two diffraction peaks is consistent with the previous report on g-C_3N_4 [35]. The XRD pattern of composite materials shows the appearance of ZnO and g-C_3N_4 peaks, which indicate the success of the composite materials.

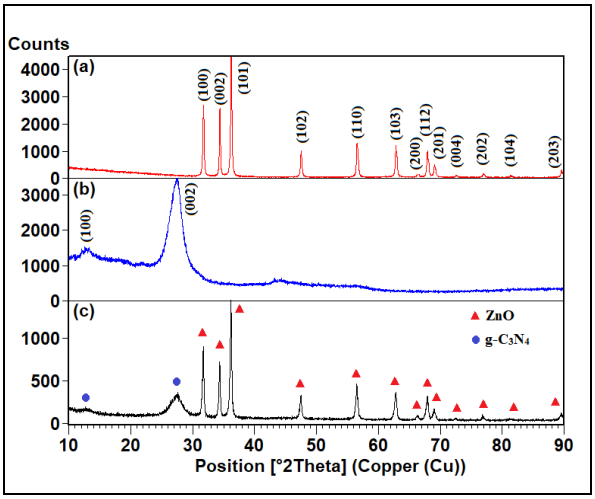

Figure 1. XRD patterns of (a) ZnO (b) g-C_3N_4 (c) g-C_3N_4/ZnO

Figure 2 represents the FESEM micrograph of pristine g-C_3N_4, pristine ZnO, and composite g-C_3N_4/ZnO at 50 k magnification. The composition of g-C_3N_4/ZnO was investigated by elemental mapping, as shown in Figure

3. (a)–(e) that confirms the uniform distribution of elements. The elements present in the material were determined using EDX analysis, as demonstrated in Figure 3 (f). The existence of Zn, O, C, and N elements can be clearly visualized in the EDX spectrum of the g-C_3N_4/ZnO, and no other elements were detected, which confirms its purity. Figure 4 (a) indicates the TEM image of g-C_3N_4/ZnO, which shows a nanospherical shape with an average crystallite size of 35 nm. The high-resolution and SAED images of g-C_3N_4/ZnO are shown in Figure 4 (b), which indicates the interplanar spacing of about 0.281 nm at the (100) plane of ZnO that is estimated from the intensity profile image.

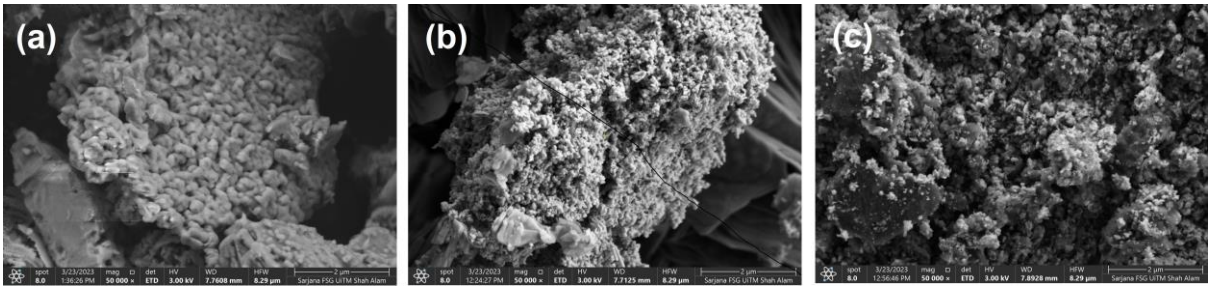

Figure 2. FESEM image of (a) g-C_3N_4 (b) ZnO (c) g-C_3N_4/ZnO at 50k magnification

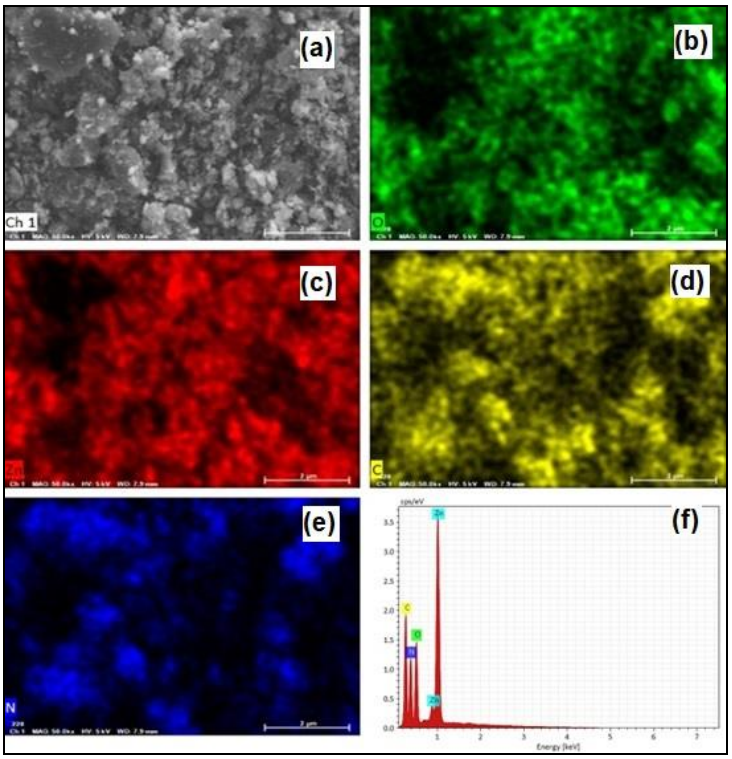

Figure 3. (a) FESEM image and elemental mapping (b) oxygen (c) zinc (d) carbon (e) nitrogen and (f) EDX spectrum of g-C_3N_4/ZnO

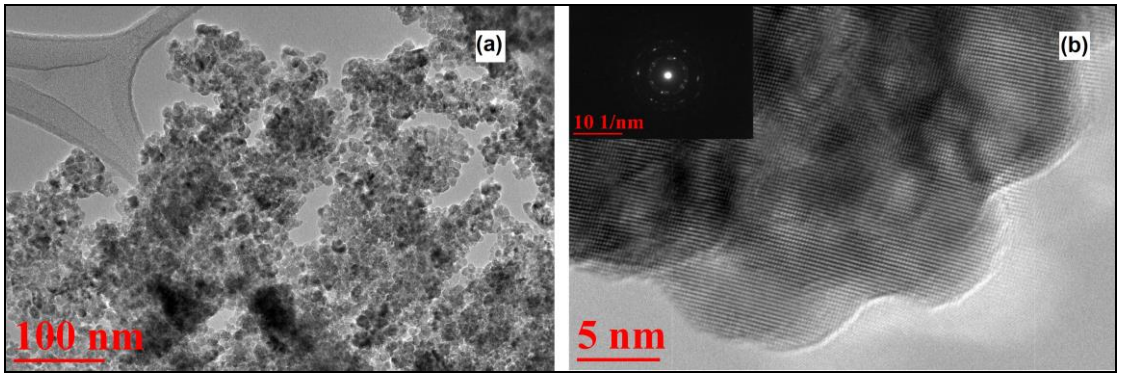

Figure 4. (a) TEM image of g-C_3N_4/ZnO at 100k magnification (b) High resolution image of g-C_3N_4/ZnO and SAED image at (100) plane

Figure 5 represents the UV-Vis reflectance spectra of ZnO, g-C_3N_4, and g-C_3N_4/ZnO. As can be observed, the composite materials exhibit the red shift towards the visible light region. Tauc plot for ZnO, g-C_3N_4, and g-C_3N_4/ZnO calculated based on the equations (2) to (4) [36]. From the reflectance spectra, a tauc plot was drawn, and the values of the band gaps can be obtained.

$$(\alpha h\upsilon) = A(h\upsilon - E_g)^n \qquad (2)$$

where α is the absorption coefficient of the material corresponding to a value of wavelength λ, h is Planck's constant, A is the proportionality constant, n is the frequency of light, E_g is the band energy, and n = ½ (for direct transition mode materials). The absorption coefficient is evaluated using equation (3):

$$\alpha = k \ln\left(\frac{R_{max} - R_{min}}{R - R_{min}}\right) \qquad (3)$$

where k is a constant, R_{max} is the maximum reflectance and R_{min} is the minimum reflectance. Consideration of equations. (2) and (3) gives equation (4),

$$(\alpha h\upsilon)^2 = A'(h\upsilon - E_g) \qquad (4)$$

where A′ is a constant. From Equation (4), a tauc plot can be drawn of $(\alpha h\nu)^2$ versus hν as shown in Figure 6. The point of the extrapolation of the linear part that meets the abscissa gives the value of the band gap energy of the material. It was found that the calculated band gap of ZnO is 3.31 eV. The band gap of g-C_3N_4 prepared is 2.81 eV whereas the band gap of g-C_3N_4/ZnO was observed to be 2.92 eV which is lower than the pristine ZnO. The reduced band gap of composite materials is attributed to the presence of g-C_3N_4 in the crystal lattice. This will cause the shifting of the valence and conduction bands, subsequently narrowing the band gap.

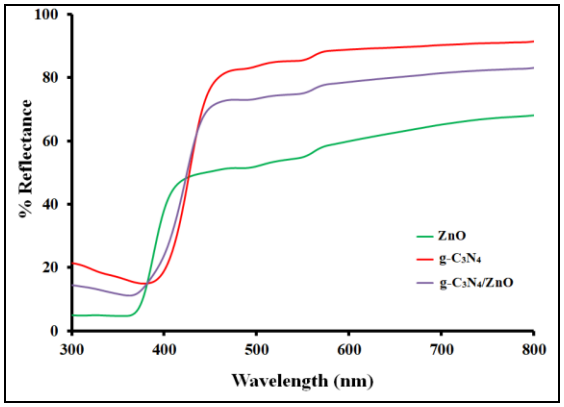

Figure 5. Reflectance spectra of ZnO, g-C_3N_4 and g-C_3N_4/ZnO

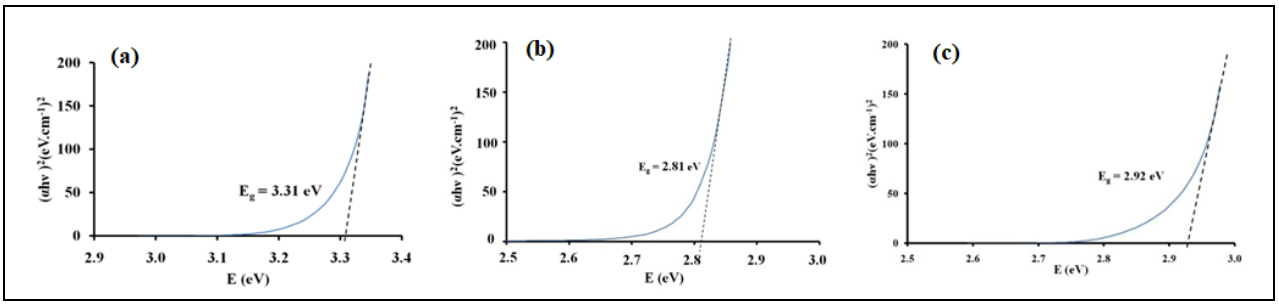

Figure 6. Tauc plot of ZnO, g-C_3N_4 and g-C_3N_4/ZnO

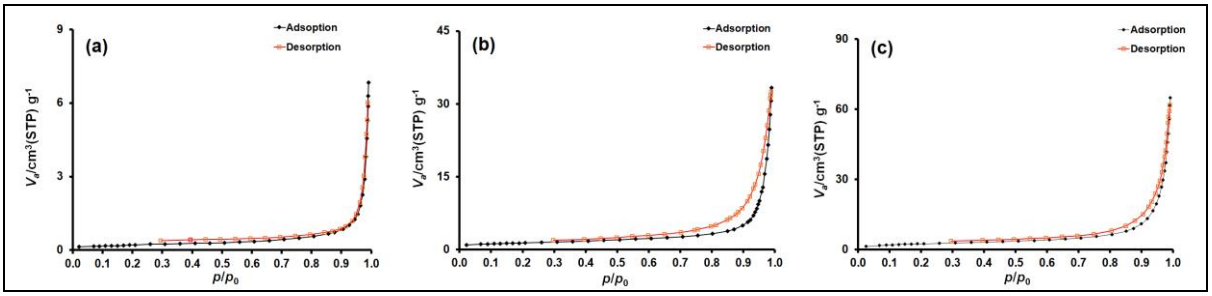

Figure 7. N_2 adsorption-desorption isotherm of (a) ZnO (b) g-C_3N_4 (c) g-C_3N_4/ZnO

Table 1 shows the values of total pore volume, pore diameter, and specific surface area of the sample from the N_2 sorption analysis as well as the percent degradation of OFL. The g-C_3N_4/ZnO had a surface area and pore volume of 8.30 m^2g^{-1} and 0.010 cm^3g^{-1}, respectively, with an average pore diameter of 46.14 nm, which is in the mesoporous range. The surface area of g-C_3N_4/ZnO is higher in comparison with that of pure g-C_3N_4. Specific surface area increases along with lower pore volume, suggesting that ZnO is loaded onto g-C_3N_4, which also enhances the photocatalytic activity [37]. The isotherm plot of g-C_3N_4/ZnO in Figure 7 shows a discerned pattern belongs to type IV and H3 hysteresis loop which represent the existence of mesoporous [38].

The percent degradation of 10 mg/L of OFL was shown in Figure 8 under irradiation of light for 180 min. The optical properties of ZnO may exhibit an absorbance potential that is suitable for the UV spectrum only, which explains the only 5.3% degradation efficiency of ZnO. The photocatalytic performance of g-C_3N_4 shows 47.9% in 180 min higher than ZnO due to the active light response in the visible light. The degradation of g-C_3N_4/ZnO is 63.4% in 180 min, which is 11 times higher than that of pristine ZnO and double than that of pristine g-C_3N_4. The reduced band gap energy of g-C_3N_4/ZnO may result in better absorption of light in the visible region, favoring more electron-hole pair formation and thus improving photocatalytic performance of g-C_3N_4/ZnO. [39]. The photocatalytic performance is influenced by the crystallinity of the photocatalyst and the surface area for both light absorption and molecule adsorption. It is shown that high surface area and pore volume of g-C_3N_4/ZnO can improve photocatalytic degradation due to a larger number of active sites that absorb and mineralize the contaminant through the inter-associated porous structure [40].

Table 1. Surface characteristics analysis and photocatalytic performance of photocatalysts

Sample	Total Pore Volume (cm^3g^{-1})	Mean Pore Diameter (nm)	Surface Area (m^2g^{-1})	Types of Pores	% Degradation
ZnO	0.009	54.10	7.22	Macroporous	5.5
g-C_3N_4	0.005	45.27	4.54	Mesoporous	47.9
g-C_3N_4/ZnO	0.010	46.14	8.30	Mesoporous	63.4

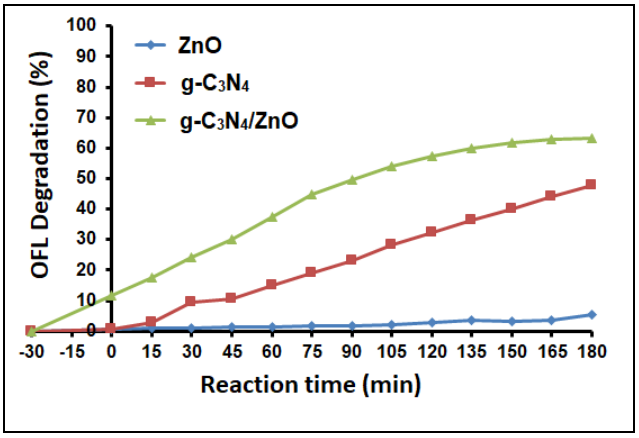

Figure 8. The percentage degradation of OFL under exposure of light at optimized condition in 180 min (Operating parameters: 0.25 g of catalyst loading, 10 mg/L concentration OFL)

Conclusion

In this work, the g-C_3N_4/ZnO photocatalyst was successfully prepared via sol-gel, thermal decomposition, and followed by impregnation methods. The prepared g-C_3N_4/ZnO photocatalyst was successfully characterized with a nanospherical shape, and a higher surface area compared to the pristine. From the band gap analysis, it was found that the band gap of g-C_3N_4/ZnO was reduced from 3.31 eV to 2.92 eV. The reduction of the band gap energy improved the performance of the photocatalytic activity in visible light. The photocatalytic activity of OFL is higher than that of pristine g-C_3N_4 and ZnO, which takes 180 min to degrade 63.4% of the OFL.

Acknowledgement

The authors would like to acknowledge the Institute of Science, Faculty of Applied Sciences, UiTM and the grant Young Talent Researcher (600-RMC/YTR/5/3 (014/2020)) for supporting this research.

References

1. Gupta, G., Kansal, S. K., Umar, A. and Akbar, S. (2023). Visible-light driven excellent photocatalytic degradation of ofloxacin antibiotic using $BiFeO_3$ nanoparticles. *Chemosphere*, 314: 137611.
2. Meng, X., Wang, Z., Li, K., Liu, Y., Zhao, D. and Fu, Y. (2023). Degradation of ofloxacin by lanthanum cerate perovskite activated bisulfite. *Environmental Technology & Innovation*, 32: 103370.
3. Zhou, G., Meng, L., Ning, X., Yin, W., Hou, J., Xu, Q., ... and Wang, X. (2022). Switching charge transfer of g-C_3N_4/$BiVO_4$ heterojunction from type II to Z-scheme via interfacial vacancy engineering for improved photocatalysis. *International Journal of Hydrogen Energy*, 47(14): 8749-8760.
4. Cipagauta-Díaz, S., Estrella-González, A., Navarrete-Magaña, M. and Gómez, R. (2022). N doped-TiO_2 coupled to $BiVO_4$ with high performance in photodegradation of Ofloxacin antibiotic and Rhodamine B dye under visible light. *Catalysis Today*, 394: 445-457.
5. Ding, C., Guo, J., Chen, P., Gan, W., Yin, Z., Qi, S., ... and Sun, Z. (2022). All-solid-state Z-scheme In_2S_3/CQDs/TiO_2 heterojunction for highly efficient degradation of ofloxacin. *Applied Surface Science*, 596: 153629.

6. Su, Q., Li, J., Yuan, H., Wang, B., Wang, Y., Li, Y. and Xing, Y. (2022). Visible-light-driven photocatalytic degradation of ofloxacin by g-C3N4/NH2-MIL-88B (Fe) heterostructure: Mechanisms, DFT calculation, degradation pathway and toxicity evolution. *Chemical Engineering Journal*, 427: 131594.
7. Zhang, M., Xu, J. and Chen, M. (2022). Novel Z-scheme $LaVO_4/Bi_3O_4Cl$ heterojunctions for highly efficient degradation of ofloxacin under visible light irradiation. *Journal of Alloys and Compounds*, 925: 166653.
8. Sharan, S., Khare, P. and Shankar, R. (2023). Electrochemical degradation of ofloxacin using PbO_2/Pb-based lead acid battery electrode: Parametric optimization and kinetics study. *Materials Today: Proceedings*, 78: 128-137.
9. Cai, H., Wang, J., Du, Z., Zhao, Z., Gu, Y., Guo, Z., ... and Fang, Y. (2023). Construction of novel ternary $MoSe_2$/ZnO/p-BN photocatalyst for efficient ofloxacin degradation under visible light. *Colloids and Surfaces A: Physicochemical and Engineering Aspects*, 663: 131050.
10. Radjenović, J., Petrović, M. and Barceló, D. (2009). Fate and distribution of pharmaceuticals in wastewater and sewage sludge of the conventional activated sludge (CAS) and advanced membrane bioreactor (MBR) treatment. *Water Research*, 43(3): 831-841.
11. Zhang, S., Wang, Y., Cao, Z., Xu, J., Hu, J., Huang, Y., ... and Wang, H. (2020). Simultaneous enhancements of light-harvesting and charge transfer in UiO-67/CdS/rGO composites toward ofloxacin photo-degradation. *Chemical Engineering Journal*, 381: 122771.
12. Ding, P., Li, J., Guo, M., Ji, H., Li, P., Liu, W., ... and Chen, S. (2023). Visible light-driven degradation of ofloxacin by graphene oxide-supported titania/zirconia ternary nanocomposites. *Inorganic Chemistry Communications*, 155: 111001.
13. Wen, Y., Wang, Z., Cai, Y., Song, M., Qi, K. and Xie, X. (2022). S-scheme BiVO4/CQDs/β-FeOOH photocatalyst for efficient degradation of ofloxacin: Reactive oxygen species transformation mechanism insight. *Chemosphere*, 295: 133784.
14. He, S., Chen, Q., Chen, G., Shi, G., Ruan, C., Feng, M., ... and Cao, C. (2022). N-doped activated carbon for high-efficiency ofloxacin adsorption. *Microporous and Mesoporous Materials*, 335: 111848.
15. Wang, X., Li, Y., Li, R., Yang, H., Zhou, B., Wang, X. and Xie, Y. (2019). Comparison of chlorination behaviors between norfloxacin and ofloxacin: reaction kinetics, oxidation products and reaction pathways. *Chemosphere*, 215: 124-132.
16. Sun, Q., Sun, Y., Zhou, M., Cheng, H., Chen, H., Dorus, B., ... and Le, T. (2022). A 2D/3D g-C_3N_4/ZnO heterojunction enhanced visible-light driven photocatalytic activity for sulfonamides degradation. *Ceramics International*, 48(5): 7283-7290.
17. Sharma, G., Kumar, A., Kumar, P. S., Alodhayb, A., ALOthman, Z. A., Dhiman, P. and Stadler, F. J. (2022). Carbon quantum dots embedded trimetallic oxide: Characterization and photocatalytic degradation of Ofloxacin. *Journal of Water Process Engineering*, 48: 102853.
18. Singh, R. and Dutta, S. (2019). The role of pH and nitrate concentration in the wet chemical growth of nano-rods shaped ZnO photocatalyst. *Nano-Structures & Nano-Objects*, 18: 100250.
19. Pirhashemi, M., Habibi-Yangjeh, A. and Pouran, S. R. (2018). Review on the criteria anticipated for the fabrication of highly efficient ZnO-based visible-light-driven photocatalysts. *Journal of Industrial and Engineering Chemistry*, 62: 1-25.
20. Sinar Mashuri, S. I., Kasim, M. F., Mohd Kaus, N. H., Yie, H. T., Islam, A., Rashid, U., ... and Ibrahim, M. L. (2023). Photo-response range extension of z-scheme ZnO/Cds for led-light-driven photo-active catalyst. *Renewable Sustainability Energy Review*, 184: 113602.
21. Lu, S., Ma, Y. and Zhao, L. (2022). Production of ZnO-CoOx-CeO_2 nanocomposites and their dye removal performance from wastewater by adsorption-photocatalysis. *Journal of Molecular Liquids*, 364: 119924.
22. Jin, C. Z., Yang, X. A., Zhai, X. M., Wang, S. B. and Zhang, W. B. (2023). ZnO/Sn_3O_4 amorphous-crystalline heterojunctions for Cr (VI) visible photocatalysis: Simple synthesis with excellent

performance. *Applied Surface Science*, 608: 155263.

23. Vo, N. T. T., You, S. J., Pham, M. T. and Van Pham, V. (2023). A green synthesis approach of p-n CuO/ZnO junctions for multifunctional photocatalysis towards the degradation of contaminants. *Environmental Technology & Innovation*, 32: 103285.
24. Akhter, P., Nawaz, S., Shafiq, I., Nazir, A., Shafique, S., Jamil, F., ... and Hussain, M. (2023). Efficient visible light assisted photocatalysis using ZnO/TiO_2 nanocomposites. *Molecular Catalysis*, 535: 112896.
25. Mohamed, M. A., Zain, M. F. M., Minggu, L. J., Kassim, M. B., Jaafar, J., Amin, N. A. S., and Ng, Y. H. (2019). Bio-inspired hierarchical hetero-architectures of in-situ C-doped g-C_3N4 grafted on C, N co-doped ZnO micro-flowers with booming solar photocatalytic activity. *Journal of Industrial and Engineering Chemistry*, 77: 393-407.
26. Wen, J., Xie, J., Chen, X. and Li, X. (2017). A review on g-C_3N_4-based photocatalysts. *Applied Surface Science*, 391: 72-123.
27. Mishra, A., Mehta, A., Basu, S., Shetti, N. P., Reddy, K. R. and Aminabhavi, T. M. (2019). Graphitic carbon nitride (g–C_3N_4)–based metal-free photocatalysts for water splitting: a review. *Carbon*, 149: 693-721.
28. Prasad, C., Tang, H. and Bahadur, I. (2019). Graphitic carbon nitride based ternary nanocomposites: From synthesis to their applications in photocatalysis: A recent review. *Journal of Molecular Liquids*, 281: 634-654.
29. Zhu, J., Xiao, P., Li, H. and Carabineiro, S. A. (2014). Graphitic carbon nitride: synthesis, properties, and applications in catalysis. *ACS Applied Materials & Interfaces*, 6(19): 16449-16465.
30. Naseri, A., Samadi, M., Pourjavadi, A., Ramakrishna, S. and Moshfegh, A. Z. (2021). Enhanced photocatalytic activity of ZnO/g-C_3N_4 nanofibers constituting carbonaceous species under simulated sunlight for organic dye removal. *Ceramics International*, 47(18): 26185-26196.
31. Mohanty, L., Pattanayak, D. S. and Dash, S. K. (2021). An efficient ternary photocatalyst Ag/ZnO/g-C_3N_4 for degradation of RhB and MG under solar radiation. *Journal of the Indian Chemical Society*, 98(11): 100180.
32. Das, D. and Nandi, P. (2022). ZnO/g-C_3N_4 heterostructures: Synthesis, characterization and application as photoanode in dye sensitized solar cells. *Solar Energy Materials and Solar Cells*, 248: 112002.
33. Zhong, Q., Lan, H., Zhang, M., Zhu, H. and Bu, M. (2020). Preparation of heterostructure g-C_3N_4/ZnO nanorods for high photocatalytic activity on different pollutants (MB, RhB, Cr (VI) and eosin). *Ceramics International*, 46(8): 12192-12199.
34. Fallahpour, M., Poursalehi, R. and Yourdkhani, A. (2023). Highly efficient photocatalytic removal of concentrated PEX, PAX and SIPX xanthates collectors by an immobilized nanostructured g-C_3N_4/ZnO low power backlighted module. *Minerals Engineering*, 204: 108416.
35. Tran, D. A., Pham, C. T. N., Ngoc, T. N., Phi, H. N., Ta, Q. T. H., Truong, D. H., and Vo, V. (2021). One-step synthesis of oxygen doped g-C_3N_4 for enhanced visible-light photodegradation of Rhodamine B. *Journal of Physics and Chemistry of Solids*, 151: 109900.
36. Kamarulzaman, N., Kasim, M. F. and Chayed, N. F. (2016). Elucidation of the highest valence band and lowest conduction band shifts using XPS for ZnO and Zn0.99Cu0.01O band gap changes. *Results in Physics*, 6: 217-230.
37. Mao, N., Jiao, Y. and Duan, X. (2022). g-C_3N_4/ZnO heterojunction as Fenton-like catalyst for degradation of organic pollution. *Materials Research Bulletin*, 151: 111818.
38. Garg, R., Gupta, R. and Bansal, A. (2021). Synthesis of g-C_3N_4/ZnO nanocomposite for photocatalytic degradation of a refractory organic endocrine disrupter. *Materials Today: Proceedings*, 44: 855-859.
39. Paul, D. R., Gautam, S., Panchal, P., Nehra, S. P., Choudhary, P. and Sharma, A. (2020). ZnO-modified g-C_3N_4: A potential photocatalyst for environmental application. *ACS Omega*, 5(8): 3828-3838.
40. Portillo-Cortez, K., Romero-Ibarra, J. E., Dominguez, D., Alonso-Nuñez, G. and Caudillo-

Flores, U. (2023). Photodegradation of ceftriaxone using g-C_3N_4-ZnO nanocomposite as an efficient photocatalyst. *Journal of Photochemistry and Photobiology A: Chemistry*, 445: 115090.